

Fractional quantum-Hall liquid spontaneously generated by strongly correlated t_{2g} electrons

Jörn W.F. Venderbos, Stefanos Kourtis, Jeroen van den Brink, and Maria Daghofer
Institute for Theoretical Solid State Physics, IFW Dresden, 01171 Dresden, Germany
(Dated: August 28, 2018)

For topologically nontrivial and very narrow bands, Coulomb repulsion between electrons has been predicted to give rise to a spontaneous fractional quantum-Hall (FQH) state in absence of magnetic fields. Here we show that strongly correlated electrons in a t_{2g} -orbital system on a triangular lattice self-organize into a spin-chiral magnetic ordering pattern that induces precisely the required topologically nontrivial and flat bands. This behavior is very robust and does not rely on fine tuning. In order to go beyond mean field and to study the impact of longer-range interactions, we map the low-energy electronic states onto an effective one-band model. Exact diagonalization is then used to establish signatures of a spontaneous FQH state.

The Integer Quantum Hall (IQH) effect [1] is a prime example of an electronic state that cannot be classified within the traditional framework of symmetry breaking, but is instead characterized by a topological invariant [2]. It is by now theoretically well established that an external magnetic field is in principle not needed and that states within the same topological class as IQH states can be realized in lattice models, if time-reversal symmetry is broken by other mechanisms, e.g., by complex electron hoppings [3]. Related topologically nontrivial Quantum Spin-Hall (QSH) states even occur in systems where time-reversal symmetry is not broken at all [4–8], see Refs. [9, 10] for reviews. At present, many intriguing features intrinsic to topologically non-trivial states have been observed in the absence of magnetic fields, such as the metallic Dirac cones at the surface of a topological insulator [11, 12], or the QSH effect in quantum wells [13, 14].

Fractional Quantum Hall (FQH) states [15] are topological states that can be seen as composed of quasi-particles carrying an exact fraction of the elementary electronic charge [16]. Apart from the fundamental interest in observing a quasi-particle that behaves in many ways like a fraction of an electron, some FQH states also have properties relevant to fault-tolerant quantum computation [17]. Very recently [18–20], it was suggested that lattice-FQH states may similarly arise without a magnetic field, in fractionally filled topologically nontrivial bands.

In contrast to the IQH and QSH effects, which can be fully understood in terms of non-(or weakly-)interacting electrons, interactions are an essential requirement for FQH states, which places demanding restrictions on candidate systems: One needs a topologically nontrivial band that must be nearly flat – similar to the highly degenerate Landau levels – so that the electron-electron interaction can at the same time be large compared to the band width and small compared to the gap separating it from other bands [18–20]. If the requirements can be fulfilled, however, the temperature scale of the FQH state is set by the energy scale of the interaction.

This can allow temperatures considerably higher than the sub-Kelvin range of the conventional FQH effect, which would be extremely desirable in view of potential quantum-computing applications. Moreover, the lattice version of FQH states [21] may have unique and different properties. [22].

In most recently proposed model Hamiltonians [18–20, 23–25], the topological nature of the bands was introduced by hand and model parameters have to be carefully tuned to obtain very flat bands. As potential realizations, “purpose built” physical systems in oxide heterostructures [26] or optical lattices [19] were suggested. On the other hand, topologically nontrivial bands can in principle emerge spontaneously in interacting electron systems [27, 28], e.g., for charge-ordered systems [29, 30] or for electrons coupling to spins in a non-coplanar magnetic order [31, 32]. We demonstrate here that such a scenario indeed arises in a Hubbard model describing electrons with a t_{2g} orbital degree of freedom on a triangular lattice: a ground state with topologically nontrivial and nearly flat bands is stabilized by onsite Coulomb interactions. Upon doping the flat bands, longer-range Coulomb repulsion induces FQH states.

t_{2g} orbitals on the triangular lattice.— The building blocks of our system are oxygen octahedra with a transition-metal (TM) ion in the center, the most common building block in the large and versatile material class of TM oxides. Local cubic symmetry due to the oxygen ions splits the d -orbitals into t_{2g} and e_g levels, and it has been shown that orbital degrees of freedom of either kind can substantially reduce the width of topologically nontrivial bands [24]. Here, we concentrate on the t_{2g} orbitals illustrated in Fig. 1(a), which are further split by a crystal-field due to the overall lattice geometry. On a triangular lattice, we find one a_{1g} and two $e'_{g,\pm}$ states, see Fig. 1(b), with a splitting $H_{JT} = \Delta_{JT}(n_{e_{g+}} + n_{e_{g-}} - 2n_{a_{1g}})/3$ depending on the Jahn-Teller effect and the lattice [33]. Electron hopping along nearest-neighbor (NN) bonds consists of terms t via ligand oxygens and t_{dd} due to direct d - d overlap [33, 34], hopping matrices are given in [35]. We set here $n < 3$ and

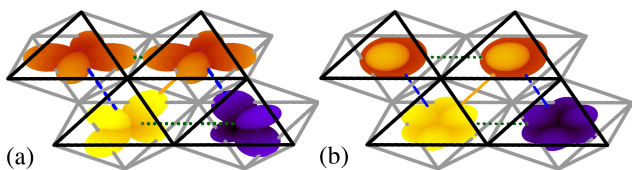


FIG. 1. (Color online) Triangular perovskite lattice and t_{2g} orbitals. Oxygen octahedra are indicated by lines, with black lines illustrating the front facets. Thick dotted (dashed, solid) lines indicate nearest-neighbor bonds along lattice vector \mathbf{a}_1 (\mathbf{a}_2 , \mathbf{a}_3). (a) Shows two d_{xy} orbitals (top) and one d_{xz} and d_{yz} orbital (bottom). In (b), the orbitals reflecting the three-fold lattice symmetry are shown: The two e'_g orbitals (bottom), which differ by their complex phases, will turn out to be half filled, while the a_{1g} orbital (pointing out of the plane, see top) forms nearly flat bands with non-trivial topological character that can support spontaneous FQH states.

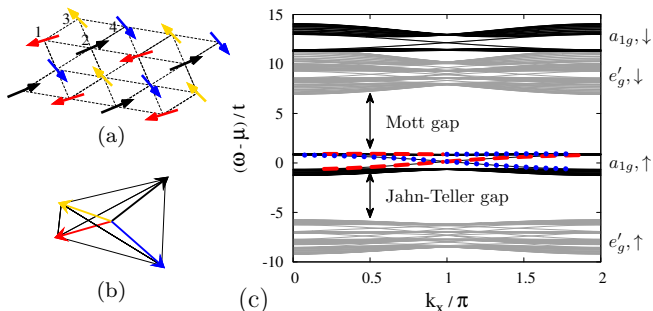


FIG. 2. (Color online) Spin-chiral magnetic phase with topologically nontrivial bands stabilized by onsite Coulomb interactions in t_{2g} electrons on a triangular lattice. (a) Chiral magnetic order, the sites of the unit cell are labeled by 1 to 4. (b) The spins on the four sites can be seen as pointing to the corners of a tetrahedron, i.e., the pattern is non-coplanar. (c) One-particle energies on a cylinder (periodic boundary conditions along x) in the mean-field [35] ground state of the t_{2g} multiorbital Hubbard model, which is given by the pattern shown in (a). States drawn in black (grey) have more (less) than 33% a_{1g} character, dashed and dotted lines indicate edge states with more than 33% of their weight on the top (bottom) row of sites. The arrows \uparrow (\downarrow) indicate states with electron spin mostly (anti-)parallel to the local quantization axis, which can be seen as the lower (upper) Hubbard band. The filling is 2.5 electrons per site, slightly less than half filling. Parameters used were $t = 1$, $t_{dd} = 0$, $U/t = 12$, $J/t = 3$, $\Delta_{JT}/t = -6$. The figure of merit M , which is given by the ratio of the gap separating the two a_{1g} subbands of the lower Hubbard band and the band width of the highest subband of the lower Hubbard band, is $M \approx 14$.

choose $t > 0$ [33] as unit of energy, but analogous results hold for $n > 3$, $t < 0$, and $t_{dd} \rightarrow -t_{dd}$, $\Delta_{JT} \rightarrow -\Delta_{JT}$ due to particle-hole symmetry.

In TM oxides, Coulomb interaction is substantial compared to the kinetic energy of t_{2g} orbitals and spin-orbital physics induced by correlations are known to be rich in t_{2g} systems on triangular lattices [34, 36]. We take into

account the onsite interaction including Coulomb repulsion U (intra-orbital) and U' (interorbital) as well as Hund's-rule coupling J . We employ a mean-field approximation with a decoupling into expectation values of densities $\langle n_{\mathbf{i},\alpha,\sigma} \rangle = \langle c_{\mathbf{i},\alpha,\sigma}^\dagger c_{\mathbf{i},\alpha,\sigma} \rangle$ for site \mathbf{i} , orbital α , and spin σ [37, 38]. The spin is thus reduced to its z -component $m_{\mathbf{i},\alpha} = (n_{\mathbf{i},\alpha,\uparrow} - n_{\mathbf{i},\alpha,\downarrow})/2$ and non-collinear magnetic patterns are treated by allowing for a site-dependent spin-quantization axis expressed by angles θ_i and ϕ_i . The change in quantization axis from site to site manifests itself in a complex Berry phase for the hopping terms [39]. Numerical optimization is used to find the θ_i and ϕ_i giving the magnetic ground state, permitting arbitrary magnetic orderings with unit cells of up to four sites, including all phases considered in Ref. [40]. For simplicity, we present here results for $J/U = 1/4$ and the relation $U' = U - 2J$ between the Kanamori parameters was used, but we have verified that the results presented remain robust for other choices. For details see [35].

For wide parameter ranges (see below), the ground state is the non-coplanar spin-chiral phase illustrated in Fig. 2(a,b). As demonstrated in the context of the Kondo-lattice [38, 40] and the Hubbard [38, 41] models, this magnetic order leads to topologically nontrivial bands, which can also be seen in the one-particle bands shown in Fig. 2(c). The chemical potential lies within the a_{1g} states of the lower Hubbard band, where the electron spin is mostly parallel (labelled by \uparrow) to the direction defined by the spin-chiral pattern. Dashed and dotted lines decorate states living on the top and bottom edges of a cylinder, they cross the chiral gap exactly once as one left- and one right-moving edge mode, indicating the different Chern numbers associated with the two bands directly above and below the chemical potential. Such a spontaneous IQH state is already rather exotic and has recently been shown to support fractionalized excitations bound to vortices [42].

Figure 2(c) also indicates that the upper chiral subband has a very small width, ~ 14 times smaller than the chiral gap. One can quantify the band flatness by a figure of merit M given by the ratio of the gap to the band width. Its dependence on various parameters of the Hamiltonian is shown in Fig. 3. It peaks at $M > 40$, but the more striking observation is that it is above 5 or even 10 for wide ranges of U , Δ_{JT} and t_{dd} , in contrast to many other proposals that require carefully fine-tuned parameters [18–20, 23–25, 43]. Nearly flat chiral bands are thus very robust in this system and both their topological character and their flat dispersion emerge spontaneously with purely onsite interaction and short-range hopping, without spin-orbit coupling or any explicit breaking of time-reversal symmetry.

Mapping to an effective model.— For large onsite interactions and large crystal field splitting $U, J, |\Delta_{JT}| \gg t, t_{dd}$, the three-orbital model with fillings between 2 and 3 electrons per site can be mapped onto the one-band

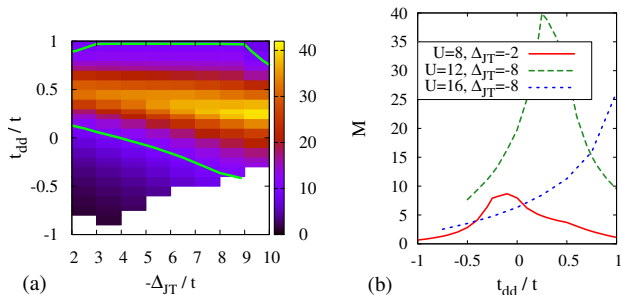


FIG. 3. (Color online) Stability of the spin-chiral phase and flatness of the topological bands depending on parameters of the Hamiltonian. In (a), shaded areas in the t_{dd} - Δ_{JT} plane indicate a spin-chiral ground state Fig. 2(a,b) for $U/t = 12$, white areas have a different ground state. Shading indicates the figure of merit M for the flatness of the upper chiral sub-band, bright thick lines bound the region with $M \geq 10$. (b) shows M depending on t_{dd} for selected sets of U and Δ_{JT} . Where the “Mott gap”, which separates the flat topologically non-trivial band from the upper Hubbard band, becomes very small, M is determined by the minimal gap separating the band of interest from other bands. $J = U/4$ and $t = 1$ were used in all cases.

Kondo-lattice model (KLM). Low-energy configurations minimize onsite interactions and thus contain two or three electrons per site, with parallel spins due to Hund’s rule. In order to additionally minimize the crystal-field energy, the e'_g levels will always be half filled and form an effective spin, while any holes will be found in the a_{1g} sector. The electrons in the partially filled a_{1g} states can delocalize with an isotropic hopping $t_{a_{1g}} = (2t + t_{dd})/3$, however, their spin must remain parallel to the local e'_g spin. In the low-energy limit, each site can thus be described as a spin coupled to a charge degree of freedom and we arrive at the situation described by the KLM in the limit of strong Hund’s rule coupling. Our numeric mean-field results corroborate this picture, see Fig. 2(c), where the e'_g levels are found far below the chemical potential. The KLM supports spin-chiral phases on many frustrated lattices like the triangular [38, 40, 44, 45], pyrochlore [46], and face-centered cubic [47] lattices.

In addition to processes within the low-energy Hilbert space, virtual excitations involving high-energy states can be taken into account in second-order perturbation theory. This leads to (i) effective longer-range hopping of the a_{1g} electrons and (ii) an effective antiferromagnetic superexchange between the e'_g spins. The latter stabilizes the spin-chiral pattern [45] and is due to excitations into the upper Hubbard/Kondo band. When it is suppressed for $U \gtrsim 24|t|$, the ground state consequently becomes FM, as in the KLM with a large Kondo gap [40, 44]. Nevertheless, the exotic spin-chiral state is remarkably stable in the present t_{2g} system considering its sensitivity to Hund’s coupling in the KLM [40].

The effective longer-range hopping of a_{1g} elec-

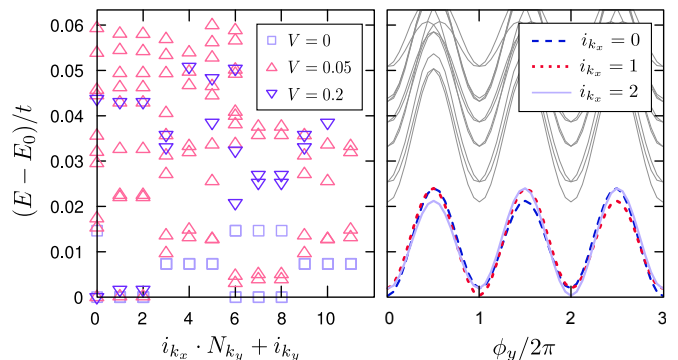


FIG. 4. (Color online) FQH state induced by NN Coulomb repulsion V in the effective one-band model Eq. 1. (a) Energy depending on total momentum \mathbf{k} for several values of V/t . (b) Energy for $V/t = 0.2$ depending on a flux ϕ_y added whenever an electron goes once around the whole lattice in y direction. Each addition of $\phi = 2\pi$ leads to an equivalent state, 6π to the same state. The Chern numbers associated with the three low-energy states are almost exactly $2/3$ for $V/t = 0.2$. Lattice size is 4×6 sites (12 two-site unit cells), parameters in Eq. 1 are $t_1 = 0.27t$ and $t_3 = -0.06t$, giving bands with $M \approx 13$ and a gap of $0.89t$. The filling of the flat band is $2/3$.

trons involves processes via excitations into the upper Kondo/Hubbard band ($\propto 1/J$ and $\propto 1/U$) as well as virtual excitations of e'_g electrons into a_{1g} states ($\propto 1/\Delta_{JT}$), for details see 35. Second-neighbor hopping $\propto 1/J$ does not significantly modify the low-energy bands and drops out completely in the limit of a large Mott/Hubbard gap, but third-neighbor hopping t_3 is crucial in cancelling the dispersion coming from NN hopping t_1 for one of the bands [35]. The simplest description of the effective low-energy bands around the Fermi level is thus

$$H_{\text{eff}}(\mathbf{k}) = 2t_1 \sum_j \sigma^j \cos \mathbf{k}\mathbf{a}_j + 2t_3 \sum_j \sigma^0 \cos 2\mathbf{k}\mathbf{a}_j, \quad (1)$$

where \mathbf{a}_j ($j = 1, 2, 3$) denote the unit vectors on the triangular lattice. Pauli matrices σ^j and unit matrix σ^0 refer to the two sites of the electronic unit cell in the chiral phase [38]. Formally, this describes electrons moving in a constant (and very strong) magnetic field with a flux of $\pi/2$ threading each triangle of the lattice [38].

FQH groundstates of an effective spinless one-band model. — We now address the impact of NN Coulomb interaction $V \sum_{\langle i,j \rangle} n_i n_j$ on the fractionally filled flat band. The spin-chiral state can only be expected to remain stable for densities close to 2.5 electrons per site, i.e., low doping fractions ν of the flat band [40]. FQH states corresponding to such low fillings are generally separated from the rest of the spectrum by only a small gap, making their analysis on finite-size clusters difficult [48]. Here, we use Lanczos exact diagonalization [20, 35, 43, 48] to study a number of simple filling fractions ($1/3$, $2/3$, $1/5$, and $2/5$) available on accessible lattices and consistently find V to induce signatures of a FQH state. It is thus plau-

sible that the FQH behavior discussed next persists to fractional fillings in a low doping range of the spin-chiral state.

As an example, we present here the case of 16 electrons on a 4×6 -site cluster of the model Eq. (1), a filling that would correspond to 2.6 in the original three-orbital model. After a particle-hole transformation, it corresponds to $2/3$ filling of the nearly flat band. Figure 4(a) shows that with increasing V , three low-energy states split off from the rest of the spectrum. Inserting a magnetic flux $\phi_y = 2\pi$ interchanges the three states, $\phi_y = 6\pi$ recovers the original situation, see Fig. 4(b), as reported for other systems [20, 24, 43]. The Chern number C is evaluated by integrating the flux-dependent Berry curvature $\Omega^n(\phi_x, \phi_y)$ (obtained by the Kubo formula [35, 49, 50]) over the square $0 \leq \phi_x, \phi_y < 6\pi$. For $V = 0.2|t|$, the three low-energy states have Chern numbers within 1% of the expected $C = 2/3$, a deviation well within the limits of reported finite-size effects [20].

Conclusions.— The possibility of a spontaneous FQH effect without a magnetic field is currently hotly discussed, and various models have been suggested [18–20, 23–26, 43]. However, an experimental realization appears challenging, as the necessary topological character and the flatness of the bands need to be carefully engineered in previous proposals. We have shown here that bands with the desired properties emerge spontaneously for wide parameter ranges in strongly correlated t_{2g} orbitals on a triangular lattice, and that these bands support FQH ground states. Both t_{2g} systems and triangular lattices occur in various TM oxides, and signatures of the unconventional *integer* QH state have been reported for a triangular-lattice palladium-chromium oxide [51]. This harbors the prospect that a suitable material can be synthesized in this highly versatile material class. As such a material is by default strongly correlated, one also naturally expects an inter-site Coulomb repulsion that is strong enough to stabilize spontaneous FQH states in the absence of a magnetic field.

This research was supported by DFG (Emmy-Noether program; SK and MD) and the Interphase Program of the Dutch Science Foundation NWO/FOM (JV and JvdB).

The appendix contains Supplemental Material:

One-particle terms of the multi-orbital t_{2g} Hamiltonian

The multi-orbital kinetic energy is

$$H_{\text{kin}} = \sum_{\langle i,j \rangle, \alpha, \beta, \sigma} t_{i,j}^{\alpha, \beta} c_{i, \alpha, \sigma}^\dagger c_{j, \beta, \sigma} + \text{H.c.}, \quad (2)$$

where $c_{i, \alpha, \sigma}^\dagger$ ($c_{i, \alpha, \sigma}$) creates (annihilates) an electron on site i , in orbital α and with spin σ . $\langle i, j \rangle$ denotes nearest-

neighbor (NN) bonds, α and β denote the orbital. Using as basis states the xy , xz , and yz orbitals shown in Fig. 1(a) of the main text, the orbital- and direction-dependent hopping parameters $t_{i,j}^{\alpha, \beta}$ are given by the matrices

$$\hat{T}_1 = \begin{pmatrix} t_{dd} & 0 & 0 \\ 0 & 0 & t \\ 0 & t & 0 \end{pmatrix}, \quad \hat{T}_2 = \begin{pmatrix} 0 & 0 & t \\ 0 & t_{dd} & 0 \\ t & 0 & 0 \end{pmatrix}, \quad \hat{T}_3 = \begin{pmatrix} 0 & t & 0 \\ t & 0 & 0 \\ 0 & 0 & t_{dd} \end{pmatrix}$$

for NN bonds along the three directions \mathbf{a}_1 , \mathbf{a}_2 , \mathbf{a}_3 as illustrated in Fig. 1 of the main text. The transformation into the $\{a_{1g}, e'_{g,+}, e'_{g,-}\}$ can be found, e.g., in Ref. [33].

Mean-field approximation

Onsite interaction is described by Kanamori parameters U (U') for Coulomb repulsion between electrons in the same (different) orbitals as well as ferromagnetic Hund's-rule coupling between electrons in different orbitals. The relation $U' = U - 2J$ is used here, ‘‘pair-hopping’’ J' is left out, because it drops out of the mean field decoupling

$$\begin{aligned} H_{\text{int}} \approx & U \sum_{\mathbf{i}, \alpha} (\langle n_{\mathbf{i}, \alpha, \uparrow} \rangle n_{\mathbf{i}, \alpha, \downarrow} + n_{\mathbf{i}, \alpha, \uparrow} \langle n_{\mathbf{i}, \alpha, \downarrow} \rangle) \\ & + (U' - J/2) \sum_{\mathbf{i}, \alpha < \beta} (\langle n_{\mathbf{i}, \alpha} \rangle n_{\mathbf{i}, \beta} + n_{\mathbf{i}, \alpha} \langle n_{\mathbf{i}, \beta} \rangle) \\ & - 2J \sum_{\mathbf{i}, \alpha < \beta} (\langle m_{\mathbf{i}, \alpha} \rangle m_{\mathbf{i}, \beta} + m_{\mathbf{i}, \alpha} \langle m_{\mathbf{i}, \beta} \rangle) \\ & - U \sum_{\mathbf{i}, \alpha} \langle n_{\mathbf{i}, \alpha, \uparrow} \rangle \langle n_{\mathbf{i}, \alpha, \downarrow} \rangle - (U' - J/2) \sum_{\mathbf{i}, \alpha < \beta} \langle n_{\mathbf{i}, \alpha} \rangle \langle n_{\mathbf{i}, \beta} \rangle \\ & + 2J \sum_{\mathbf{i}, \alpha < \beta} \langle m_{\mathbf{i}, \alpha} \rangle \langle m_{\mathbf{i}, \beta} \rangle, \end{aligned} \quad (3)$$

where \mathbf{i} labels the site, α and β orbitals. $n_{\mathbf{i}, \alpha, \sigma} = c_{\mathbf{i}, \alpha, \sigma}^\dagger c_{\mathbf{i}, \alpha, \sigma}$ is the density operator. We keep here only expectation values for diagonal operators, i.e., only $\langle n_{\mathbf{i}, \alpha, \sigma} \rangle = \langle c_{\mathbf{i}, \alpha, \sigma}^\dagger c_{\mathbf{i}, \alpha, \sigma} \rangle$ [37, 38], which reduces the spin to its z -component $m_{\mathbf{i}, \alpha} = (n_{\mathbf{i}, \alpha, \uparrow} - n_{\mathbf{i}, \alpha, \downarrow})/2$. In order to treat non-collinear spin patterns, one has to allow for a site-dependent spin-quantization axis given by angles θ_i and ϕ_i . The change in quantization axis from site to site manifests itself in a complex phase for the hopping terms, [39] which is between sites i and j

$$\begin{aligned} \Omega_{ij}^{\sigma, \sigma} &= \cos \frac{\theta_i}{2} \cos \frac{\theta_j}{2} + \sin \frac{\theta_i}{2} \sin \frac{\theta_j}{2} e^{-i\sigma(\phi_i - \phi_j)} \\ \Omega_{ij}^{\uparrow, \downarrow} &= \cos \frac{\theta_i}{2} \sin \frac{\theta_j}{2} e^{-i\phi_j} - \cos \frac{\theta_j}{2} \sin \frac{\theta_i}{2} e^{-i\phi_i} \end{aligned} \quad (4)$$

where $\Omega_{ij}^{\uparrow, \uparrow}$ ($\Omega_{ij}^{\downarrow, \downarrow}$) modulates the hopping of an electron with spin parallel (antiparallel) to the chosen spin-quantization axis. In the site-dependent quantization,

spin is not conserved and there are spin-mixing hoppings with $\Omega_{ij}^{\downarrow,\uparrow}$ given by the complex conjugate of $\Omega_{ji}^{\uparrow,\downarrow}$.

We use numerical optimization routines to find the spin pattern with the lowest energy among all orderings with unit cells of up to four sites, including all patterns considered in Ref. [40] of the main text. In each step, the mean-field energy is calculated self-consistently for a lattice of 16×16 (four-site unit cell) or 24×16 (three-site unit cell). (For selected points in parameter space, we also used larger lattices and did not find a significant difference.) In order to minimize the impact of our approximations on the symmetries of the orbital degrees of freedom, we perform the mean-field decoupling in the $\{a_{1g}, e'_{g,+}, e'_{g,-}\}$ basis, where the symmetry between the half-filled $e'_{g,+}$ and the quarter-filled a_{1g} orbitals (for the fillings discussed here) is already broken by the crystal field. We verified that decoupling directly in the $\{xy, xz, yz\}$ basis, where all three orbitals have the same electronic density, leads to qualitatively identical and quantitatively very similar results.

Effective one-band model and exact diagonalization

The mapping to the effective one-band model is most easily carried out in the Kondo-lattice picture, where the localized spins are assumed to consist of the e'_g electrons. Without a magnetic order, the a_{1g} orbital has an isotropic hopping $t_{a_{1g}} = (2t + t_{dd})/3$, i.e., the same along all three directions on the triangular lattice, but in the spin-chiral phase, this hopping is modulated by a direction-dependent Berry phase Eq. (4). The electronic unit cell of the spin-chiral pattern has two sites [38], and the Berry phases can then be expressed in terms of Pauli matrices as given in the main text. The absolute value of the NN hopping is renormalized to $t_1 = (2t + t_{dd})/3\sqrt{3}$.

Corrections to this simplest approximation can be obtained by second-order perturbation theory, which yields longer-range hopping processes mediated by virtual excitations. We are first going to discuss processes within the lower Kondo/Hubbard band, where an electron from the e'_g levels, which are half filled in the low-energy Hilbert space, is excited into an empty a_{1g} state in the virtual intermediate state, involving an excitation energy Δ_{JT} . In a second step, an electron from a different *occupied* a_{1g} state can take the empty place in the e'_g orbital, which corresponds to an effective hopping. There are two possible hopping paths connecting pairs of either nearest or next-nearest neighbor (NNN) sites and it turns out that the corresponding effective hoppings drop out in the spin-chiral phase because the Berry phases for the two paths interfere destructively. Third-neighbor sites, on the other hand, are only connected by a single path and the combined Berry phase $\Omega_{ij}^{\uparrow,\uparrow}\Omega_{jk}^{\uparrow,\uparrow}$ only renormalizes the effective hopping by a factor of 3, because the spins at sites i and k are parallel in the spin-chiral phase. One thus

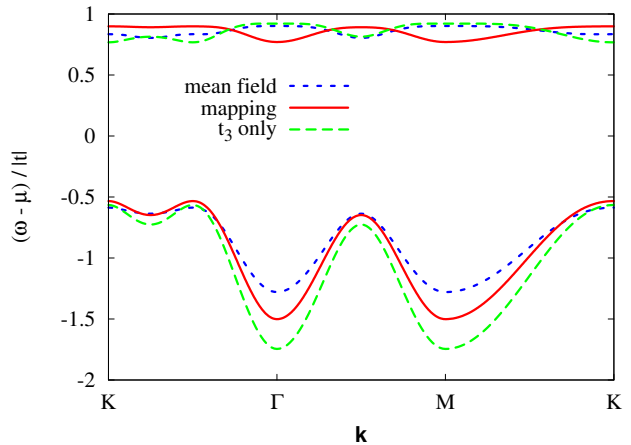


FIG. 5. (Color online) Comparison of the low-energy bands obtained in mean field theory for the spin-chiral state to those obtained in the strong-coupling Kondo-lattice model, including effective hoppings in second-order perturbation theory. Parameters in mean field are $U/t = 12$, $J/t = 3$, $\Delta_{JT}/t = -6$, and $t_{dd} = 0$, as in Fig. 2 of the main text. The different dispersions in the upper band are due to the fact that the perturbation theory assumes that the second-order-hopping path is always available. As the a_{1g} level is partly filled, some of these paths are blocked by the Pauli principle, this effect is included correctly in mean field. Taking this into account phenomenologically by reducing t_3 by 20% improves the fit. This was done for the curve referred to as “ t_3 only”, where only nearest and third-neighbor hopping were included, while second-neighbor processes were dropped.

obtains an effective hopping $t_3 = -2(t - t_{dd})^2 / (27\Delta_{JT})$, which is the only second-order correction for the limit of infinite Hund’s rule. In this limit, t_3 flattens the *lower* of the subbands for the fillings discussed here [24].

In the more realistic case of strong but finite Hund’s rule coupling, there are additional processes where the virtual excitation involves an electron in the upper Hubbard/Kondo band. The corresponding excitation energies then contain Hund’s coupling J and the effective hoppings from site i to k involve the Berry phases $\Omega_{ij}^{\downarrow,\downarrow}\Omega_{jk}^{\downarrow,\downarrow}$, see Eq. (4). For the parameters of Fig. 2 of the main text, the chiral bands around the Fermi level are compared to this second-order treatment in Fig. 5. NNN hopping does here not drop out, and NN hopping is also slightly renormalized, however, both these processes have only a small impact on the low-energy bands. Again, we find third-neighbor hopping t_3 to flatten the dispersion of one of the bands. Since excitations into the upper Hubbard/Kondo band involve *electrons* rather than holes as before, the sign of the effective t_3 is reversed, and it is the upper chiral subband that is flattened.

In order to investigate the FQH groundstate, we used Lanczos exact diagonalization to study the Hamiltonian given by the kinetic energy of the effective one-band model, Eq. (1) of the main text, and NN Coulomb repul-

sion $V \sum_{\langle i,j \rangle} n_i n_j$. Hopping parameters $t_1 = 0.27$ and $t_3 = -0.058$ were used, giving a dispersion similar to Fig. 5. NN bonds $\langle i,j \rangle$ are defined on the original triangular lattice and V acts both between the two sites within one unit cell and between NN sites belonging to different unit cells. As mentioned in the main text, the spin-chiral state can actually only be expected to be stable for low doping of the flat band [40], which is close to half filling for the effective one-band model. FQH states corresponding to such small fillings ν tend to have smaller gaps than those for large ν , and the low-energy manifold giving the quasi-degenerate FQH states contains more states. On the small clusters that we can study with exact diagonalization, eigenenergies always have spacings between them, as an illustration see the $V = 0$ energies in Fig. 4(a) of the main text, which would form a continuous band in the thermodynamic limit. It is thus far harder to reliably resolve a small gap than a larger one, and it is moreover highly desirable that we can study the system on at least two lattice sizes in order to see a gap. This severely restricts our access to very low dopings. We thus study several filling fractions corresponding to “simple” FQH states. In all cases where we find a low-energy manifold to separate from the rest of the spectrum, the states of this low-energy manifold shows signatures of

FQH behavior, which is thus a very robust feature of the doped flat band.

Inserting a flux (ϕ_x, ϕ_y) means that electrons gain a phase $e^{i\phi_x}$ ($e^{i\phi_y}$) for going once around the whole lattice in x -(y -) direction. This is implemented by changing the hopping $t_{i,j}$ from site $\mathbf{i} = i_x \mathbf{a}_1 + i_y \mathbf{a}_2$ to site $\mathbf{j} = j_x \mathbf{a}_1 + j_y \mathbf{a}_2$ to

$$t_{i,j} \rightarrow t_{i,j} e^{i\left(\phi_x \frac{j_x - i_x}{L_x} + \phi_y \frac{j_y - i_y}{L_y}\right)}, \quad (5)$$

leading to a flux-dependent Hamiltonian $H_{\text{eff}}(\phi_x, \phi_y)$. In the case of $\nu = 1/3$, we find three low-energy states separated from the remaining spectrum by a gap as in the $\nu = 2/3$ case discussed in the main text, both on a 6×6 and a 4×6 system. For 6×6 sites, however, all three low-energy states have total momentum $(0, 0)$ for $(\phi_x, \phi_y) = (0, 0)$. Due to finite-size effects, the states do then not cross upon flux insertion [48], but avoid crossings. For the smaller 4×6 system, the three low-energy states have different total momenta, and this good quantum number allows us to clearly resolve their crossing when we insert a flux ϕ_y , even on a finite system.

The Chern numbers were evaluated by integrating the Berry curvature $\Omega^n(\phi_x, \phi_y)$ over the square $0 \leq \phi_x, \phi_y < 6\pi$. $\Omega^n(\phi_x, \phi_y)$ was obtained by the Kubo formula [49, 50]

$$\Omega^n(\phi_x, \phi_y) = iL_x L_y \sum_{n' \neq n} \frac{\langle n | \frac{\partial H_{\text{eff}}(\phi_x, \phi_y)}{\partial \phi_x} | n' \rangle \langle n' | \frac{\partial H_{\text{eff}}(\phi_x, \phi_y)}{\partial \phi_y} | n \rangle - \langle n | \frac{\partial H_{\text{eff}}(\phi_x, \phi_y)}{\partial \phi_y} | n' \rangle \langle n' | \frac{\partial H_{\text{eff}}(\phi_x, \phi_y)}{\partial \phi_x} | n \rangle}{(\epsilon_n - \epsilon_{n'})^2}, \quad (6)$$

where n' and n label eigenstates with energies $\epsilon_{n'}/n$ and $\partial H_{\text{eff}}(\phi_x, \phi_y)/\partial \phi_{x/y}$ are current operators.

-
- [1] K. v. Klitzing, G. Dorda, and M. Pepper, Phys. Rev. Lett. **45**, 494 (1980).
 - [2] D. J. Thouless, M. Kohmoto, M. P. Nightingale, and M. den Nijs, Phys. Rev. Lett. **49**, 405 (1982).
 - [3] F. D. M. Haldane, Phys. Rev. Lett. **61**, 2015 (1988).
 - [4] C. L. Kane and E. J. Mele, Phys. Rev. Lett. **95**, 146802 (2005).
 - [5] L. Fu, C. L. Kane, and E. J. Mele, Phys. Rev. Lett. **98**, 106803 (2007).
 - [6] R. Roy, Phys. Rev. B **79**, 195322 (2009).
 - [7] J. E. Moore and L. Balents, Phys. Rev. B **75**, 121306 (2007).
 - [8] B. A. Bernevig and S.-C. Zhang, Phys. Rev. Lett. **96**, 106802 (2006).
 - [9] M. Hasan and C. Kane, Rev. Mod. Phys. **82**, 3045 (2010).
 - [10] X.-L. Qi and S.-C. Zhang, Rev. Mod. Phys. **83**, 1057 (2011).
 - [11] H. Zhang, C.-X. Liu, X.-L. Qi, X. Dai, Z. Fang, and

-
- S.-C. Zhang, Nature Phys. **5**, 438 (2009).
 - [12] Y. Xia, D. Qian, D. Hsieh, L. Wray, A. Pal, H. Lin, A. Bansil, D. Grauer, Y. S. Hor, R. J. Cava, and M. Z. Hasan, Nature Phys. **5**, 398 (2009).
 - [13] B. A. Bernevig, T. L. Hughes, and S.-C. Zhang, Science **314**, 1757 (2006).
 - [14] M. König, S. Wiedmann, C. Brüne, A. Roth, H. Buhmann, L. W. Molenkamp, X.-L. Qi, and S.-C. Zhang, Science **318**, 766 (2007).
 - [15] D. C. Tsui, H. L. Stormer, and A. C. Gossard, Phys. Rev. Lett. **48**, 1559 (1982).
 - [16] R. B. Laughlin, Phys. Rev. Lett. **50**, 1395 (1983).
 - [17] C. Nayak, S. H. Simon, A. Stern, M. Freedman, and S. Das Sarma, Rev. Mod. Phys. **80**, 1083 (2008).
 - [18] E. Tang, J.-W. Mei, and X.-G. Wen, Phys. Rev. Lett. **106**, 236802 (2011).
 - [19] K. Sun, Z. Gu, H. Katsura, and S. D. Sarma, Phys. Rev. Lett. **106**, 236803 (2011).
 - [20] T. Neupert, L. Santos, C. Chamon, and C. Mudry, Phys. Rev. Lett. **106**, 236804 (2011).
 - [21] X.-L. Qi, Phys. Rev. Lett. **107**, 126803 (2011).
 - [22] M. Barkeshli and X.-L. Qi, arXiv:1112.3311.
 - [23] X. Hu, M. Kargarian, and G. A. Fiete, Phys. Rev. B **84**, 155116 (2011).
 - [24] J. W. Venderbos, M. Daghofer, and J. van den Brink,

- Phys. Rev. Lett. **107**, 116401 (2011).
- [25] Y.-F. Wang, Z.-C. Gu, C.-D. Gong, and D. N. Sheng, Phys. Rev. Lett. **107**, 146803 (2011).
- [26] D. Xiao, W. Zhu, Y. Ran, N. Nagaosa, and S. Okamoto, Nature Comm. **2**, 596 (2011).
- [27] S. Raghu, X.-L. Qi, C. Honerkamp, and S.-C. Zhang, Phys. Rev. Lett. **100**, 156401 (2008).
- [28] K. Sun, H. Yao, E. Fradkin, and S. A. Kivelson, Phys. Rev. Lett. **103**, 046811 (2009).
- [29] G. A. Fiete, V. Chua, X. Hu, M. Kargarian, R. Lundgren, A. Ruegg, J. Wen, and V. Zyuzin, arXiv:1106.0013.
- [30] S. Nishimoto, M. Nakamura, A. O'Brien, and P. Fulde, Phys. Rev. Lett. **104**, 196401 (2010).
- [31] P. Matl, N. Ong, Y. Yan, Y. Li, D. Studebaker, T. Baum, and G. Doubinina, Phys. Rev. B **57**, 10248 (1998).
- [32] Y. Taguchi, Y. Oohara, H. Yoshizawa, N. Nagaosa, and Y. Tokura, Science **291**, 2573 (2001).
- [33] W. Koshibae and S. Maekawa, Phys. Rev. Lett. **91**, 257003 (2003).
- [34] H. F. Pen, J. van den Brink, D. I. Khomskii, and G. A. Sawatzky, Phys. Rev. Lett. **78**, 1323 (1997).
- [35] See Supplemental Material.
- [36] B. Normand and A. M. Oleś, Phys. Rev. B **78**, 094427 (2008).
- [37] T. Nomura and K. Yamada, J. Phys. Soc. Jpn. **69**, 1856 (2000).
- [38] I. Martin and C. D. Batista, Phys. Rev. Lett. **101**, 156402 (2008).
- [39] E. Dagotto, *Nanoscale Phase Separation and Colossal Magnetoresistance* (Berlin: Springer, 2002).
- [40] Y. Akagi and Y. Motome, J. Phys. Soc. Jpn. **79**, 083711 (2010).
- [41] T. Li, arXiv:1103.2420.
- [42] R. A. Muniz, A. Rahmani, and I. Martin, arXiv:1112.3347.
- [43] D. N. Sheng, Z.-C. Gu, K. Sun, and L. Sheng, Nature Comm. **2**, 389 (2011).
- [44] Y. Kato, I. Martin, and C. D. Batista, Phys. Rev. Lett. **105**, 266405 (2010).
- [45] S. Kumar and J. van den Brink, Phys. Rev. Lett. **105**, 216405 (2010).
- [46] G.-W. Chern, Phys. Rev. Lett. **105**, 226403 (2010).
- [47] R. Shindou and N. Nagaosa, Phys. Rev. Lett. **87**, 116801 (2001).
- [48] N. Regnault and B. A. Bernevig, arXiv:1105.4867.
- [49] Q. Niu, D. Thouless, and Y.-S. Wu, Phys. Rev. B **31**, 3372 (1985).
- [50] D. Xiao, M.-C. Chang, and Q. Niu, Rev. Mod. Phys. **82**, 1959 (2010).
- [51] H. Takatsu, S. Yonezawa, S. Fujimoto, and Y. Maeno, Phys. Rev. Lett. **105**, 137201 (2010).